

## OPEN ACCESS

EDITED BY  
Carlos Sacristán Yagüe,  
Centro de Investigación en Sanidad Animal  
(CISA), Spain

REVIEWED BY  
Ioannis A. Giantsis,  
University of Western Macedonia, Greece  
Carmelo Iaria,  
University of Messina, Italy

\*CORRESPONDENCE  
Francesca Carella  
✉ francesca.carella@unina.it

RECEIVED 06 August 2023  
ACCEPTED 13 November 2023  
PUBLISHED 13 December 2023

CITATION  
Carella F, Prado P, De Vico G, Palić D, Villari G,  
García-March JR, Tena-Medialdea J, Cortés  
Melendreras E, Giménez-Casaldueiro F,  
Sigovini M and Aceto S (2023) A widespread  
picornavirus affects the hemocytes of the  
noble pen shell (*Pinna nobilis*), leading to its  
immunosuppression.  
*Front. Vet. Sci.* 10:1273521.  
doi: 10.3389/fvets.2023.1273521

COPYRIGHT  
© 2023 Carella, Prado, De Vico, Palić, Villari,  
García-March, Tena-Medialdea, Cortés  
Melendreras, Giménez-Casaldueiro, Sigovini  
and Aceto. This is an open-access article  
distributed under the terms of the [Creative  
Commons Attribution License \(CC BY\)](#). The use,  
distribution or reproduction in other forums is  
permitted, provided the original author(s) and  
the copyright owner(s) are credited and that  
the original publication in this journal is cited, in  
accordance with accepted academic practice.  
No use, distribution or reproduction is  
permitted which does not comply with these  
terms.

# A widespread picornavirus affects the hemocytes of the noble pen shell (*Pinna nobilis*), leading to its immunosuppression

Francesca Carella<sup>1\*</sup>, Patricia Prado<sup>2</sup>, Gionata De Vico<sup>1</sup>,  
Dušan Palić<sup>3</sup>, Grazia Villari<sup>1</sup>, José Rafael García-March<sup>4</sup>,  
José Tena-Medialdea<sup>4</sup>, Emilio Cortés Melendreras<sup>5</sup>,  
Francisca Giménez-Casaldueiro<sup>6</sup>, Marco Sigovini<sup>7</sup> and  
Serena Aceto<sup>1</sup>

<sup>1</sup>Department of Biology, University of Naples Federico II, Naples, Italy, <sup>2</sup>Institute of Agrifood Research and Technology (IRTA)-Sant Carles de la Ràpita, Tarragona, Spain, <sup>3</sup>Chair for Fish Diseases and Fisheries Biology, Faculty of Veterinary Medicine, Ludwig-Maximilians-University Munich, Munich, Germany, <sup>4</sup>Instituto de Investigación en Medio Ambiente y Ciencia Marina, Universidad Católica de Valencia, Calpe, Spain, <sup>5</sup>Murcia University Aquarium, University of Murcia, Murcia, Spain, <sup>6</sup>Department of Marine Science and Applied Biology, Research Marine Centre in Santa Pola (CIMAR), University of Alicante, Alicante, Spain, <sup>7</sup>Consiglio Nazionale delle Ricerche, Istituto di Scienze Marine, Venice, Italy

**Introduction:** The widespread mass mortality of the noble pen shell (*Pinna nobilis*) has occurred in several Mediterranean countries in the past 7 years. Single-stranded RNA viruses affecting immune cells and leading to immune dysfunction have been widely reported in human and animal species. Here, we present data linking *P. nobilis* mass mortality events (MMEs) to hemocyte picornavirus (PV) infection. This study was performed on specimens from wild and captive populations.

**Methods:** We sampled *P. nobilis* from two regions of Spain [Catalonia (24 animals) and Murcia (four animals)] and one region in Italy [Venice (6 animals)]. Each of them were analyzed using transmission electron microscopy (TEM) to describe the morphology and self-assembly of virions. Illumina sequencing coupled to qPCR was performed to describe the identified virus and part of its genome.

**Results and discussion:** In 100% of our samples, ultrastructure revealed the presence of a virus (20 nm diameter) capable of replicating within granulocytes and hyalinocytes, leading to the accumulation of complex vesicles of different dimensions within the cytoplasm. As the PV infection progressed, dead hemocytes, infectious exosomes, and budding of extracellular vesicles were visible, along with endocytic vesicles entering other cells. The THC (total hemocyte count) values observed in both captive (eight animals) ( $3.5 \times 10^4$ – $1.60 \times 10^5$  ml<sup>-1</sup> cells) and wild animals (14 samples) ( $1.90$ – $2.42 \times 10^5$  ml<sup>-1</sup> cells) were lower than those reported before MMEs. Sequencing of *P. nobilis* (six animals) hemocyte cDNA libraries revealed the presence of two main sequences of *Picornavirales*, family *Marnaviridae*. The highest number of reads belonged to animals that exhibited active replication phases and abundant viral particles from transmission electron microscopy (TEM) observations. These sequences correspond to the genus *Sogarnavirus*—a picornavirus identified in the marine diatom *Chaetoceros tenuissimus* (named *C. tenuissimus* RNA virus type II). Real-time PCR performed on the two most abundant RNA viruses previously identified by *in silico* analysis revealed positive results only for sequences similar to the *C. tenuissimus* RNA virus. These results may not conclusively identify picornavirus in noble pen shell hemocytes; therefore, further study is required. Our findings

suggest that picornavirus infection likely causes immunosuppression, making individuals prone to opportunistic infections, which is a potential cause for the MMEs observed in the Mediterranean.

#### KEYWORDS

immunosuppression, mass mortality, noble pen shell, RT-PCR, RNA virus

## 1 Introduction

Since June 2016, thousands of the noble pen shell *Pinna nobilis* individuals have died in the Mediterranean due to an extensive mass mortality event (MME) (1–7). The wide geographic range of the phenomenon makes the mass mortality of the species one of the largest known marine wildlife epizootic mortality events to date in the Mediterranean Sea (2, 8). The event was first observed along hundreds of kilometers of the southeastern coast of the Iberian Peninsula (9). Mass mortalities were subsequently observed in the northwestern Mediterranean (French and Italian coasts) and soon after in Greece, Cyprus, Turkey, Algeria, Tunisia, Morocco, Albania, and Croatia (1–5). The cause of this MME has been attributed to different pathogens, particularly *Haplosporidium pinnae* and *Mycobacterium* spp. (10–12). The presence of a great variety of pathogens associated with MMEs, including several potentially opportunistic pathogens, suggests that disease pathogenesis leading to animal mortality may have other unidentified causes (4, 13).

The order *Picornavirales* comprises positive-strand RNA viruses ranging between 7,000 and 12,500 nt in length (14). Within this order, the family *Picornaviridae* comprises 29 genera (<https://ictv.global/report/chapter/picornaviridae/picornaviridae>) of picornaviruses (PVs) (15). Picornaviruses are small, icosahedral viruses with single-stranded, highly diverse positive-sense RNA genomes associated with mild to severe diseases in vertebrates, invertebrates, and plants (16–18). The family *Picornaviridae* includes some of the most important groups in the development of virology, comprising poliovirus, rhinovirus, and hepatitis A virus (18, 19).

Virions consist of a capsid with no envelope surrounding a core of ssRNA measuring 22–33 nm in diameter (14, 20, 21). Next-generation sequencing (NGS) has significantly expanded the order *Picornavirales* in recent years through the identification of previously unknown viruses associated with various taxa, including aquatic vertebrates and invertebrates (22–27). The replication cycle takes place in the cytosol in close association with reorganized cytoplasmic membranous structures (28, 29). Infection with PV can induce numerous changes in infected cells, with the massive accumulation of cytosolic double-membraned vesicles (DMVs) and replication organelles possibly being the most important changes (30–32). Picornaviruses target intracellular membranes to generate complex membrane rearrangements of host organelles, such as the endoplasmic reticulum (ER), mitochondria, or endolysosomes (33, 34). Host intracellular membranes contain molecules, lipids, and proteins that serve as vehicles for intercellular communication in various (patho)physiological processes (35). The membrane may

provide optimal platforms for viral RNA synthesis by concentrating viral replicative proteins and relevant host factors, as well as hiding replication intermediates, contributing to the evasion of host innate immune sensors (36).

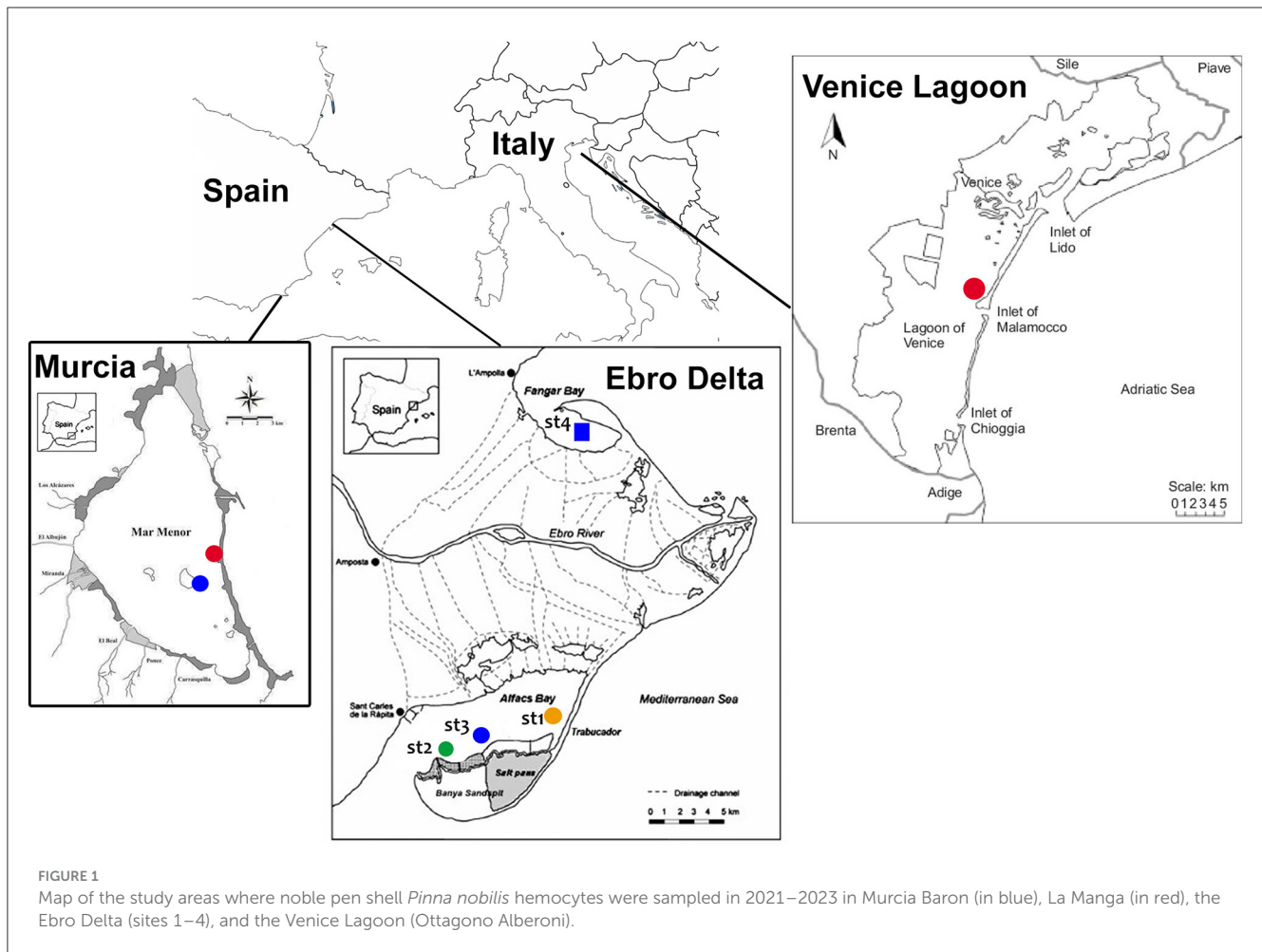
Here, we report the discovery of a previously undescribed picornavirus infecting the immune cells of the noble pen shell *Pinna nobilis* sampled between 2021 and 2023 in different regions of Spain and Italy, where mortality events have been reported. Thirty specimens were analyzed using transmission electron microscopy (TEM) to describe the morphology and self-assembly of virions within the hemocyte cytoplasm and major structural transformations occurring in infected host cells. Illumina sequencing coupled to qPCR was performed to describe the identified virus and part of its genome.

## 2 Materials and methods

### 2.1 Hemolymph collection and investigation of viral agents in hemocytes

Due to its status as an endangered species, sampling of *P. nobilis* was carried out with the permission of regional and national authorities for animal welfare (for Spain, Generalitat de Catalunya—Identificació de l'expedient: SF/0003/23; Bank of species of the Mar Menor INF/2020/0017 promoted by the General Directorate of the Mar Menor and the University of Murcia; for Italy, Prot. MATTM 0016478 05/03/2020). A total of 30 animals were included in the study, collected from July 2021 to May 2023. Sampling was performed on natural populations along the Mediterranean coasts of Italy ( $n = 4$ ) and Spain ( $n = 18$ ) and on animals maintained in captivity in two facilities in Spain ( $n = 8$ ). The natural sites in Spain and Italy were selected according to the presence of remaining populations of *P. nobilis*, despite the occurrence of mortality outbreaks (Figure 1).

In Catalonia (Spain), samples were collected from two estuarine populations in the Ebro Delta, where residual populations still exist: Fangar Bay (northern hemidelta) and Alfacs Bay (southern hemidelta), which are distributed in four different monitored areas (28). Mortality was first observed in 2018, leaving only a few individuals by 2021 (37). The mortality rate progressively increased from 33.5% in September 2021 to 75% in June 2023 (Prado pers. comm). Some of the remaining animals from this area are maintained in the aquarium facilities of the Instituto de Investigación en Medio Ambiente y Ciencia Marina (IMEDMAR) of the Universidad Católica de Valencia (UCV), in Valencia, Spain, and were included in the study. Another remaining population in



Spain is the one located at the Mar Menor lagoon (Murcia), in the southwestern part of the Mediterranean. In this area, *P. nobilis* mortality was first observed in the summer of 2016. Initially, the *P. nobilis* mortality was correlated with an environmental collapse that became critical in 2016, 2019, and 2021 and reduced the population by >99% (38); for the present work, two surviving localities were sampled in the Baron and La Manga areas (39); some animals ( $n = 2$ ) from this area were transferred to the seawater tanks of the University of Murcia Aquarium. Animals ( $n = 6$ ) had been kept in captivity at IMEDMAR and Murcia Aquarium facilities for 6 months to 1 year. Until recently, *P. nobilis* was widely distributed in the Venice Lagoon (Italy), with the largest and densest colonies over marine tidal deltas and the outer part of central basins (40). Mortality onset was observed at the end of 2020, when the population decreased between 60 and 80% (unpublished data). The animals ( $n = 4$ ) were sampled near Ottogono Aberoni Island, approximately 1 km away from the Malamocco inlet (Sigovini, personal communication).

For each animal included in the study (from the field and in captivity), 2 ml of hemolymph was collected via a 23-gauge needle from the posterior adductor muscle as a non-destructive sampling. The presence of clinical signs of disease was considered during sampling. Previous reports in the literature indicate that outward signs of disease start with behavioral changes, including

shell gaping, slow valve closure speed when touched, and mantle retraction into the valves from the edge of the shell (11). These signs were difficult to recognize in animals in the field and those maintained in captivity since they mostly appear at very late stages of disease (11). In Catalonia, on July 21 and July/August 2022, most of the animals in the study (19) displayed apparent slow valve closure. In Venice Lagoon, in May 2023, animals displayed quick valve closure and visible mantle at the border of the valves instead. Nevertheless, 2 months later, remarkable mortality was observed in the sampling area. Animals maintained in the Murcia Aquarium and IMEDMAR-UCV did not show apparent signs of disease, but in both cases, up to 40–60% of the animals suffered sudden mortality in the following 6 months, primarily attributed to manipulation from artificial spawning attempts.

After the procedure, the animals were immediately relocated to the seabed/tanks, and their health was monitored over the following days. A volume of ~2 ml of hemolymph was collected for each animal. A 1 ml hemolymph aliquot was placed in a 1 ml RNA Later (Sigma-Aldrich, Italy)-labeled tube placed on ice for molecular analyses, and the other half was preserved for ultrastructural analyses. A small hemolymph aliquot (20  $\mu$ l) was placed on a hemocytometer (Burker chamber) to determine the total cell number ( $\times 10^5$ /ml) and define the total hemocyte count (THC) (Table 1).

TABLE 1 List of collected samples of noble pen shell *P. nobilis* hemolymph in the Mediterranean Sea.

Site	Month and year	Number of collected animals evaluated by TEM	Sample type	Mean THC ( $\text{ml}^{-1}$ ) of collected animals over the years
Alfacs site 1 Trabucador	July 2021 July 2022	6	Hemolymph	(4 in 2021): $2.35 \pm 0.82 \text{ cells} \times 10^5$ (2 in 2022): $1.90 \pm 0.33 \text{ cells} \times 10^5$
Alfacs site 2 Xiringuito	July 2021 July 2022	5	Hemolymph	(3 in 2021): $2.42 \pm 0.42 \text{ cells} \times 10^5$ (2 in 2022): $2.15 \pm 0.34 \text{ cells} \times 10^5$
Alfacs site 3 Barca	July 2021 August 2022	4	Hemolymph	(3 in 2021) $2.30 \pm 1.0 \text{ cells} \times 10^5$ 2022 n.a.
Fangar site 4	May 2023	3	Hemolymph	n.a.
Murcia aquarium	September 22	4	Hemolymph	$1.60 \pm 0.22 \text{ cells} \times 10^5$
Tanks of IMEDMAR-UCV	July 21 May 2023	6	Hemolymph	(4 in 2021): $7.9 \pm 0.3 \text{ cells} \times 10^4$ (2 in 2023) $3.5 \pm 0.3 \text{ cells} \times 10^4$
Venice lagoon	May 2023	6	Hemolymph	n.a.

The number of samples analyzed per year is indicated in parentheses. n.a., data not available; THC, total hemocyte count.

## 2.2 Transmission electron microscopy

For all the animals included in the study, part of the hemolymph was also fixed in 2.5% glutaraldehyde in PBS for 3 h. Cells were postfixed in 1% osmium tetroxide for 60 min and 0.25% uranyl acetate overnight. The cells were then dehydrated through a graded ethanol series and embedded in EPON resin overnight at 37°C, 1 day at 45°C, and 1 day at 60°C. Ultrathin sections (80 nm) were cut parallel to the substrate and placed onto a 200-mesh copper grid. Bright-field TEM images were obtained on the dried sample by using an FEI TECNAI G2 200 kV s-twin microscope operating at 120 kV (Thermo Fisher Scientific, Waltham, USA). Digital images were acquired with an Olympus VELETA camera.

## 2.3 RNA extraction, sequencing, and bioinformatic analysis

Total RNA was extracted from the hemocytes of six samples of *P. nobilis* collected from three sites of the wild population in Alfacs Bay, Catalonia (Table 2) using the PureLink RNA Mini Kit (Thermo Fisher Scientific, Waltham, Massachusetts, USA). Following DNase treatment, RNA concentration and quality were measured using a Nanodrop 2000 spectrophotometer (Thermo Fisher Scientific). Strand-specific cDNA libraries were prepared, and Illumina sequencing (NovaSeq 6000, 150 bp paired-end) was carried out by Eurofins Genomics (Ebersberg, Germany). Raw reads underwent trimming and adapter clipping using Trimmomatic 0.4 (41).

To identify RNA viruses eventually infecting the *P. nobilis* hemocytes, the trimmed, good-quality reads were aligned to the *P. nobilis* genome (ASM1616189v1) using Bowtie2 (42), and the unmapped reads were extracted using SAMtools (43).

A total of 33,097,808 paired unmapped reads were assembled using Trinity 2.12.0 (44), and the abundance estimation of contigs was performed with RSEM (45).

The Trinity-assembled contigs (140,922) were used as queries in a BLASTX search against the viral protein database (<https://ftp.ncbi.nlm.nih.gov/refseq/release/viral/>, downloaded on 6 June 2023). To focus the annotation on RNA viruses, the assembled contigs were analyzed using Virsorter2 (46) by selecting only the classification of RNA viruses. Additionally, VirBot, an RNA viral contig detector for metagenomic data (47), was utilized with the sensitive option. The contigs identified as positive by both VirSorter2 and VirBot were subjected to analysis using ORFfinder (<https://www.ncbi.nlm.nih.gov/orffinder/>). The resulting ORFs were then subjected to a BLASTP search against the UniProtKB/Swissprot, RefSeq protein, and non-redundant protein sequence databases on 4 July 2023.

The predicted sequences of the RNA-dependent RNA polymerase (RdRp) protein encoded by the identified RNA viruses were used for BLASTP searches against the viral protein database, and the highest scoring homologous sequences were downloaded. Multiple amino acid alignments of the selected RdRp sequences were performed using the Constraint-based Multiple Alignment Tool (COBALT, [https://www.ncbi.nlm.nih.gov/tools/cobalt/re\\_cobalt.cgi](https://www.ncbi.nlm.nih.gov/tools/cobalt/re_cobalt.cgi)). The best amino acid substitution model was searched, and the maximum likelihood tree was generated using the LG + G + I model and 500 bootstrap replicates using MEGAX (48), resulting in a final dataset of 317 characters.

## 2.4 Quantitative real-time PCR to detect the presence of the virus in *Pinna* hemocytes

Total RNA was extracted from the hemocytes of other 5 animals *P. nobilis* samples collected from different areas in Alfacs

TABLE 2 Samples of the noble pen shell *P. nobilis* used to extract RNA from hemocytes and raw data sequencing statistics.

Sample ID	Collection place	Collection date	Sequenced reads	Sequenced bases
Bar1	Alfacs Bay site 3	August 2022	25,189,100	7,556,730,000
Bar2	Alfacs Bay site 3	August 2022	28,331,700	8,499,510,000
Trab8a	Alfacs Bay site 1	July 2022	27,304,600	8,191,380,000
Trab8b	Alfacs Bay site 1	July 2022	29,977,200	8,993,160,000
Xir2a	Alfacs Bay site 2	July 2022	27,649,600	8,294,880,000
Xir5a	Alfacs Bay site 2	July 2022	23,687,100	7,106,130,000

TABLE 3 Samples of the noble pen shell *P. nobilis* used to extract RNA from hemocytes used for qPCR.

Sample ID	Collection place	Collection date
Bar6	Alfacs Bay site 3	August 2022
Bar7	Alfacs Bay site 3	August 2022
Trab3	Alfacs Bay site 1	July 2022
Trab5	Alfacs Bay site 1	July 2022
Xir6	Alfacs Bay site 2	July 2022

Bay, Catalonia (Table 3), as described before. RNA (500 ng) was reverse-transcribed using Maxima First Strand cDNA Synthesis (Thermo Scientific). Specific primer pairs were designed to amplify the two most abundant RNA viruses identified by the *in silico* analysis (Table 4), and quantitative real-time PCR experiments were conducted. Amplification reactions were performed in a total volume of 10  $\mu$ l using 5  $\mu$ l of PowerUp SYBR Green Master Mix (Applied Biosystems), 0.2  $\mu$ M of each specific primer, and adjusted to 10  $\mu$ l with distilled water. The reactions were conducted in technical duplicates using *P. nobilis* elongation factor-1 (*EF-1*) as a reporter gene (49, 50) (Table 4). The amplification conditions were as follows: 1 cycle for 2 min at 50°C; 1 cycle for 2 min at 95°C; 40 cycles of amplification at 95°C for 15 s; 60°C for 18 s; and 72°C for 1 min. The reactions were conducted in the QuantStudio 3 Real-Time PCR System (Thermo Scientific). The cDNA of the samples identified as Trab8a and XIR2a (the same used in the RNA-seq experiment) was subjected to real-time PCR amplification to confirm the results of the *in silico* analysis, and two negative controls were run without cDNA.

## 3 Results

### 3.1 Total hemocyte count, ultrastructure of infected hemocytes, and virus details

The THC values varied among individuals and areas over the years. The mean hemocyte count showed the lowest values from animals maintained in captivity in the IMEDMAR-UCV and Murcia Aquarium (between  $3.5 \times 10^4$  and  $1.60 \times 10^5$  ml<sup>-1</sup> cells) compared with those from the natural population in Catalonia ( $1.90$ – $2.42 \times 10^5$  ml<sup>-1</sup> cells) (Table 1). The most represented cells were granulocytes ( $\sim 10$   $\mu$ m), displaying a small peripheral nucleus,

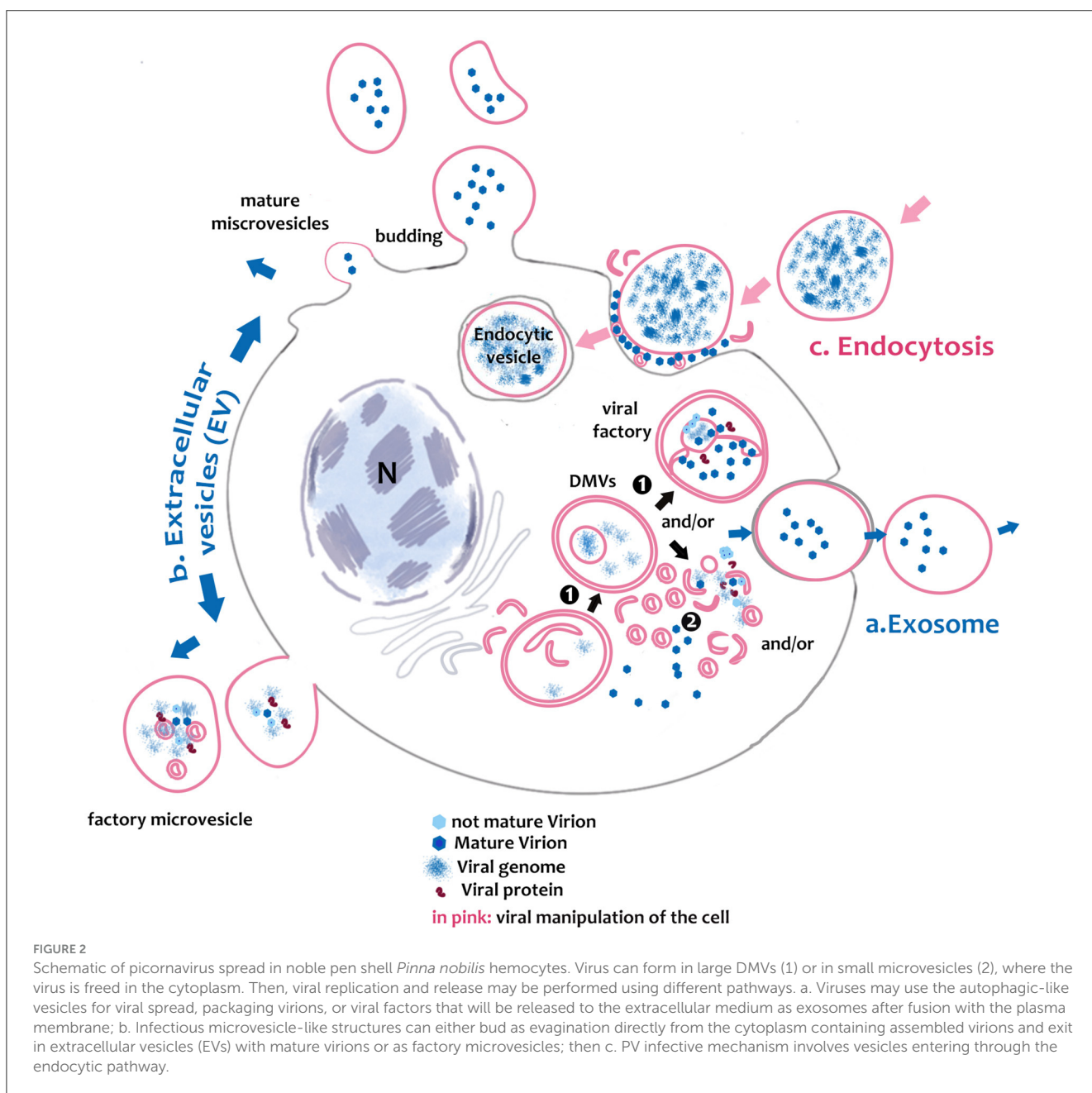
and a small quantity of hyalinocytes ( $\sim 7$   $\mu$ m), presenting a large central nucleus and small cytoplasm. All the hemocytes collected from animals in all areas of Italy and Spain from 2021 to 2023 (100%) displayed ultrastructural features of viral infection with associated cell death. These hemocytes all exhibited complex and unique membrane relocations, displaying numerous cytoplasmic vesicles associated with damaged mitochondria, a total lack of granules, the presence of protein aggregates, and, in some cases, cellular buddings. The formation of invaginations occurred at the membrane of various organelles, including the ER, endolysosomes, and mitochondria (Figures 2, 3). Features of viral infection at the hemocyte level are represented in Figure 2.

In all immune cells, aggregates of modified membranes occupied large areas of the perinuclear cytoplasm. Numerous membranous vesicles forming virions at various stages of self-assembly were visible. Vesicles in the cytoplasm were clearly associated with a dilated ER and nuclear membrane (Figures 3C, D). These vesicles had different dimensions and were constituted by double membranes, reported in the literature as DMVs or as autophagosome-like vesicles. The small vesicles measured 80–100 nm, whereas larger DMVs measured  $\sim 800$ – $1,000$  nm (Figures 3C–E). The presence of viral particles related to cytoplasmic vesicles, or mitochondrial membranes, was visible in all immune cells of *P. nobilis* (Figure 3F). Smaller vesicles were mostly used for virus genome replication at the cytoplasmic level, whereas larger DMVs supported a later step of virus production, specifically provirion maturation and the formation of complex factories. The DMVs displayed evident double or more complex membranes (Figure 4A). In earlier phases, the DMVs were filled by an unassembled viral amorphous and granular material; vesicles then showed one or two ring-like structures captured in the lumen vesicle, as also reported in other PVs (34) (Figure 4B). Viral replication factories are typically constituted by complex membrane remodeling emerging from DMVs formed by viral particles and proteins assembling mature virions, in some cases packed together. The virion is an icosahedral, non-enveloped, small (20 nm) particle with no discernible projections (Figures 4C, D).

Once the virus is assembled, viral release can occur through different mechanisms. Viruses can be released without lysis through so-called secretory autophagy, which occurs after the fusion of DMVs with the plasma membrane and are released as exosomes. Exosome typical dimensions ranged between 800 and 1,000 nm. Exosomes were secreted after their fusion with cell membrane vesicles and released as single-membraned virus-filled vesicles (Figures 4E, F). The four samples from Venice Lagoon, defined

TABLE 4 Primers used for the assessment of virus presence in noble pen shell *Pinna nobilis* hemocytes.

Primer	Sequence	Amplicon length (bp)	Reference seq accession number	Primer position on reference seq
PNChetoF	AGGGATGTTTGTGGGAGCAC	193	OR448788	5,561–5,580
PNChetoR	ACGCCGAGGGTATTCTACT			5,753–5,734
PNPicornF	CGTCCGATGCCTCTCACTAC	167	OR448789	5,702–5,721
PNPicornR	AACCGGTCGAGCCAAGAAAT			5,868–5,849
EF1bivF	CTGGGKTKTGGACAAACTGAAG	211	XM_034472995.1	299–320
EF1bivR	GATACCAGCTTCAAATTCACCA			509–488



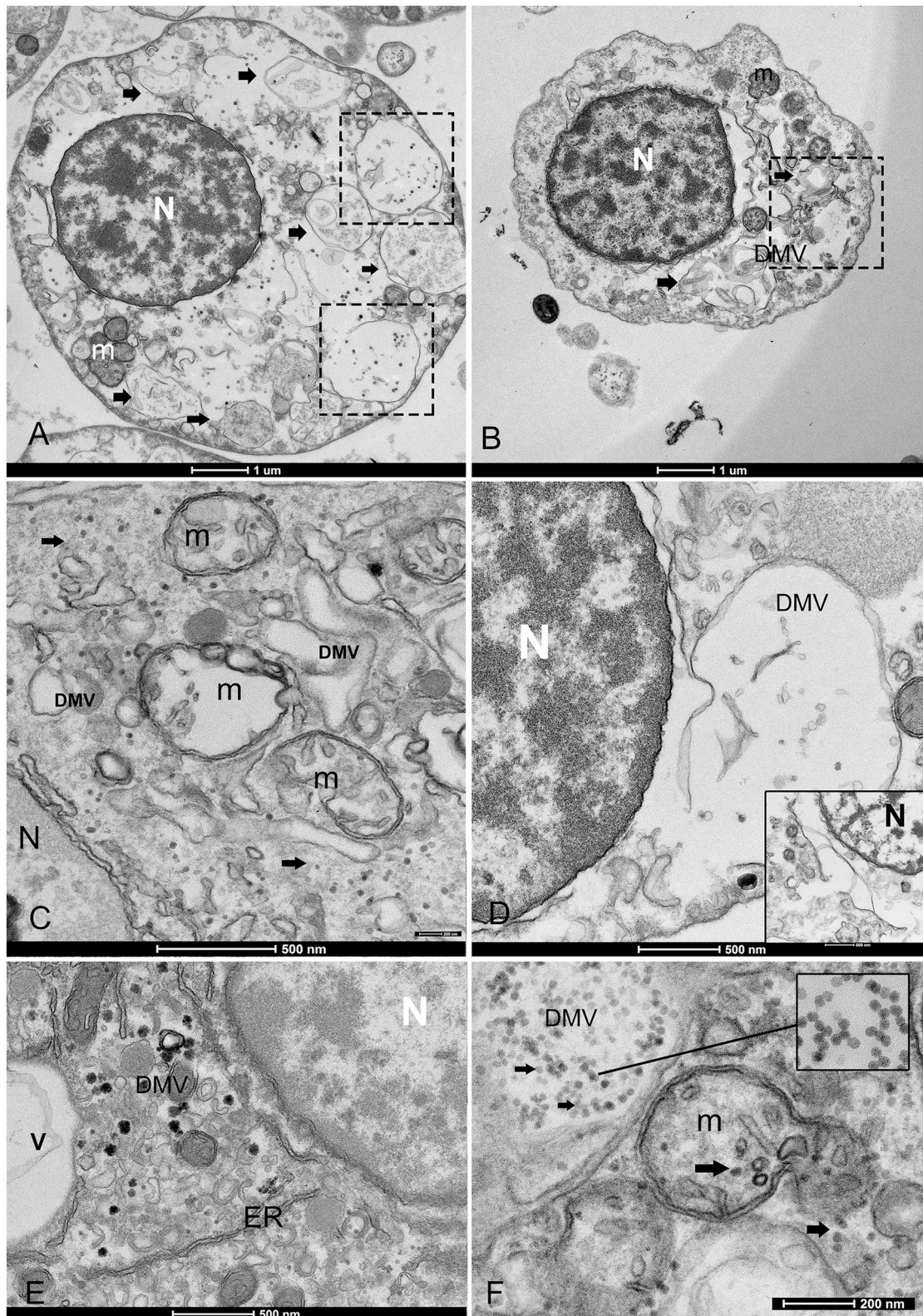
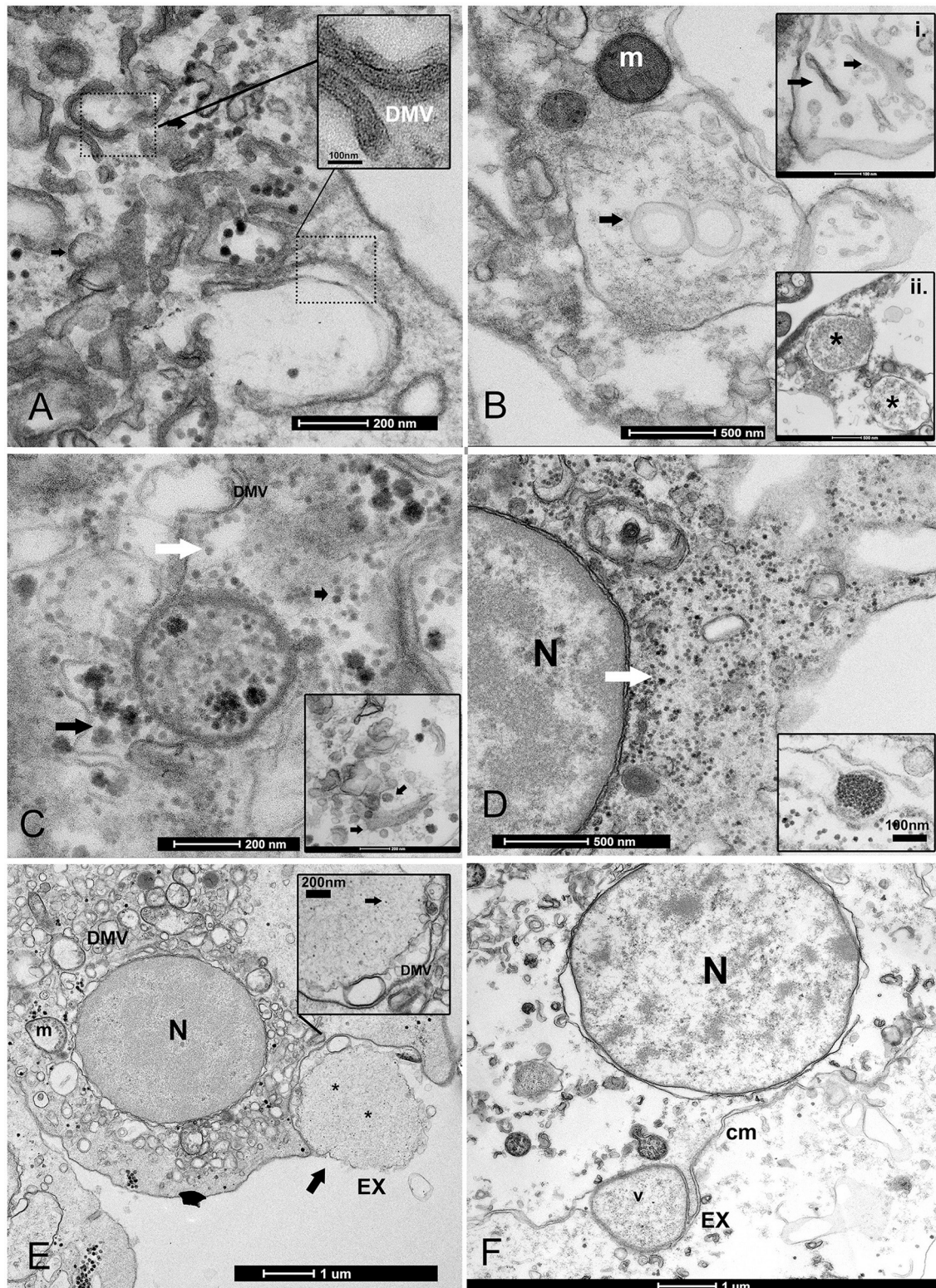


FIGURE 3

Overview of the morphological features of viral infection in the hemocytes of noble pen shell *Pinna nobilis*. (A, B) Granulocytes (A) and hyalinocytes (B) displaying double-membrane vesicles (DMVs) (arrows and squares). (C) Small vesicles (100–200 nm DMVs) and damaged mitochondria (m) with visible presence of viral particles in the cytoplasm (arrows); (D) Vesicle originates from the ER and nuclear membrane (inset); (E) Endoplasmic reticulum (ER) rearranged, forming DMV (v) and detail of zippered ER that consists of long stretches of ER-derived paired membranes. (F) Detail of vesicles containing viral particles (inset) and virus replication in a mitochondrion (m) but also present in the cell free in the cytoplasm (arrows). N, nucleus.



**FIGURE 4**

Biogenesis of double-membrane vesicles (DMVs) and exosome vesicles during PV replication. **(A)** Details of small and large DMVs with densely packed membranes that have an active role in viral RNA synthesis. **(B)** DMV biogenesis requires several membrane-remodeling steps: the biogenesis of DMVs can occur by the induction of positive membrane curvature through membrane pairing (inset i); these structures form cisternae that curve to finally seal and transform into a closed DMV and form ring-like vesicles, as reported in other picornaviruses where viral material can assemble (inset ii); **(C, D)** The virus replicates into factories through remodeled double membranes (inset), producing mature virions (white arrow) that accumulate in these large intracellular compartments from immature and forming ones (black arrow). **(D)** PV spreading into the granulocyte cytoplasm (white arrow); inset: grouped mature virions into vesicles. **(E, F)** Vesicles filled with viral particles (\*) are released into the extracellular medium as exosomes (EX) after fusion with the cell membrane; viral egress involves the fusion of a double-membrane vesicle (V) with the cell membrane (CM); N, nucleus; m, mitochondria.

in the field as apparently healthy, displayed mature viral particles spreading into the cytoplasm (Figure 4D), small DMVs, and active factories.

The predominant infective strategy observed in the PV of *P. nobilis*, typical for non-enveloped viruses, was a non-lytic “unconventional secretion” using extracellular vesicles (EVs) (Figure 5). PV-infected cells secreted EVs carrying viral RNA particles. Vesicles ranged in diameter from 100 to 700 nm. Virions may be released from cells by a budding process from both granulocytes and hyalinocytes (Figures 5A–C). Infective vesicles were observed carrying either mature viral particles (Figure 5D) or vesicle factories containing still immature virions and DMVs (Figures 5E, F). EVs may be taken up by recipient cells by endocytosis or fusion with the plasma membrane. The vesicle is internalized, via endocytosis, in an endocytic vacuole surrounded by DMVs to form mature viral particles (Figures 6A, B). Infective vesicles transporting mature virions and injecting their contents were also visible (Figures 6C, D).

Dead hemocytes were observed during infections. The highest number of damaged cells was observed in animals maintained in captivity at IMEDMAR-UCV and Murcia Aquarium, surrounded by an elevated number of EVs or containing endocytic vesicles. Damaged cells appeared empty, shrunk, contained few vesicles, and presented membrane rupture and apoptotic bodies (Figure 7).

### 3.2 Identification of RNA viruses in *P. nobilis* hemocytes

Sequencing of six stranded cDNA libraries retrieved from hemocyte samples of six *P. nobilis* using Illumina technology generated a total of 162,139,300 paired-end raw reads (Table 2), subsequently deposited in the NCBI Sequence Read Archive (SRA) under the BioProject accession PRJNA999583. After trimming and mapping against the *P. nobilis* genome, the number of unmapped paired reads was 33,097,808 (20.4%). These unmapped reads were used to assemble the viral RNA genomes present in the *P. nobilis* hemocytes.

BLASTX analysis of the 140,922 contigs assembled using Trinity resulted in 61,634 positive matches (43.7%, e-value <10<sup>-20</sup>) against the viral protein database, encompassing DNA and RNA viruses as well as bacteriophages. Since this study was performed to identify RNA viruses in *P. nobilis* hemocytes, we focused specifically on this viral group using VirSorter2 and VirBot software tools. Both analyses identified the same set of five contigs, ranging from 5,210 to 8,876 nucleotides (nt) in length, all classified, with a score of 1 (the highest possible score with VirSorter2), into the realm *Riboviria*.

These five sequences exhibited the highest BLASTX matches with different *Riboviria* polyproteins 1 and 2 (Table 5), mainly of *Picornavirales*. Notably, two of these contigs (TRINITY\_DN35348\_c1\_g1 and TRINITY\_DN9545\_c0\_g1) displayed the highest number of mapped reads, particularly in the Trab samples (Site 1, Trabucador), indicating their abundance among the five identified viruses. Additionally, during the global BLASTX analysis, we discovered the contig

TRINITY\_DN58105\_c0\_g1\_i1 (841 nt), which matched the predicted replication-associated protein of *Chaetoceros tenuissimus* RNA virus type II (BAP99820.1). Manual overlap with TRINITY\_DN35348\_c1\_g1 (5,210 nt, matched with the predicted structural protein of *Chaetoceros tenuissimus* RNA virus type II, BAP99821.1) resulted in a 6,023 nt consensus sequence.

Figure 8 presents the genomic organization of the two most prevalent viruses identified herein. The sequence consensus\_DN35348\_c1\_g1\_DN58105\_c0\_g1 (A) is partial, lacking the complete 5'-end, while the DN9545\_c0\_g1 sequence (B) is complete. These two sequences were deposited in GenBank under accessions OR448788 and OR448789. The ORFfinder analysis identified two large ORFs encoding two viral polyproteins in both sequences. Within polyprotein 1, there were conserved domains of RdRp and RNA helicase (the latter was detected only in sequence DN9545). In contrast, structural polyproteins 2 have two rhv-like domains (picornavirus capsid protein domain-like), a CRPV capsid domain (a family of capsid proteins found in positive stranded ssRNA viruses), and a short VP4 domain (a family of minor capsid proteins located within the viral capsid at the interface between the external protein shell and packaged RNA genome). The presence of two large ORFs encoding these specific domains suggests that these viral sequences belong to the *Picornavirales* order.

The genomic organization of the remaining three viruses identified in *P. nobilis* hemocytes found herein (DN33054, DN37302, and DN33329) was deposited in GenBank under accession numbers OR448790, OR448791, and OR448792, respectively (Supplementary Figure 1). Similar to the two most abundant viruses, the genomic organization of DN33054 and DN37302 presented two large ORFs, with ORF1 encoding RdRp and RNA helicase and ORF2 encoding two rhv-like domains, a CRPV capsid domain and a short VP4 domain. In contrast, the genomic organization of DN33329 was quite different, with three partially overlapping main ORFs encoding a peptidase and RdRp, similar to the structure of the *Sobelivirales* order.

The maximum likelihood tree was generated based on the alignment of the conserved region of the RdRp proteins of the viruses identified in the *P. nobilis* hemocytes with homologous sequences downloaded from GenBank (Figure 9). Almost all of the RdRp sequences downloaded from GenBank belonged to *Picornavirales* from marine or freshwater environmental samples. A restricted number of sequences belonged to *Sobelivirales*, and two of them (*Penaeus vannamei* picornavirus and Wenzhou shrimp virus 8) to *Dicistoviridae*, which are associated with mollusk and crustacean diseases (27, 51). Among the viral sequences identified in *P. nobilis* hemocytes, DN33329 clustered with those in the order *Sobelivirales*, along with viruses from rivers, soil, and plants, agreeing with the genomic organization previously described (Supplementary Figure 1). Additionally, the remaining four sequences from *P. nobilis* belonged to the order *Picornavirales*, as expected from their genomic organization; among them, the two most abundant were clustered within the family *Marnaviridae*.

In terms of ultrastructure, both samples from the Trabucador area (Trab8a and Trab8b) that had the highest number of mapped viral reads displayed numerous cytoplasmic viral factories and

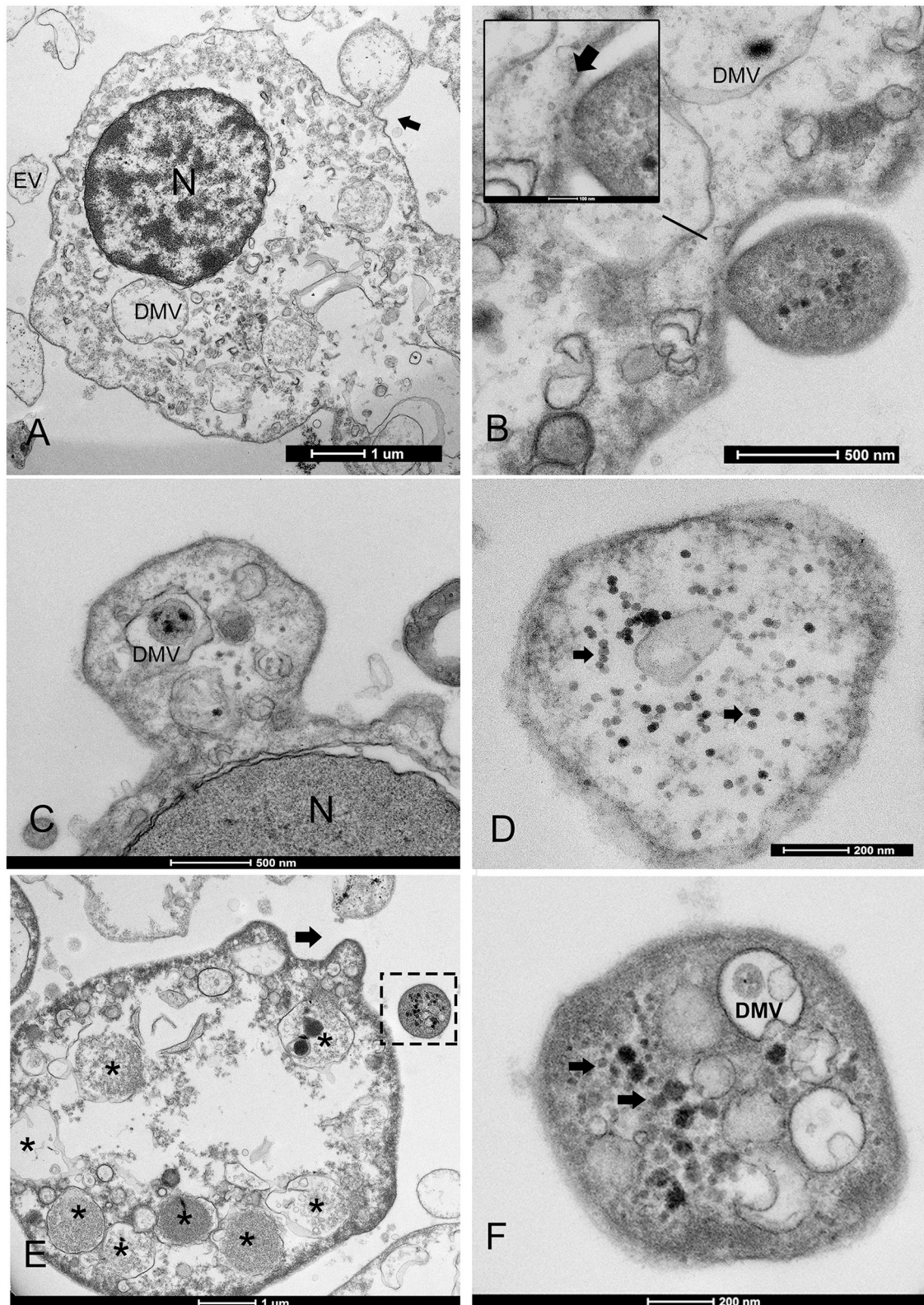


FIGURE 5

Extracellular vesicle (EV) formation during PV infection. (A, B) The EV lipid membrane mediates the release of virions through budding formation (arrow) with shedding microvesicles. (B) Details of budding from the cell membrane (arrow). (C) Hyalocyte budding formation; (D) Vesicles might contain mature virions (arrows) or viral and/or host factor viral components (\*) and induced/alter host factors (E, F); N, nucleus; DMV, double-membrane vesicles within the EV.

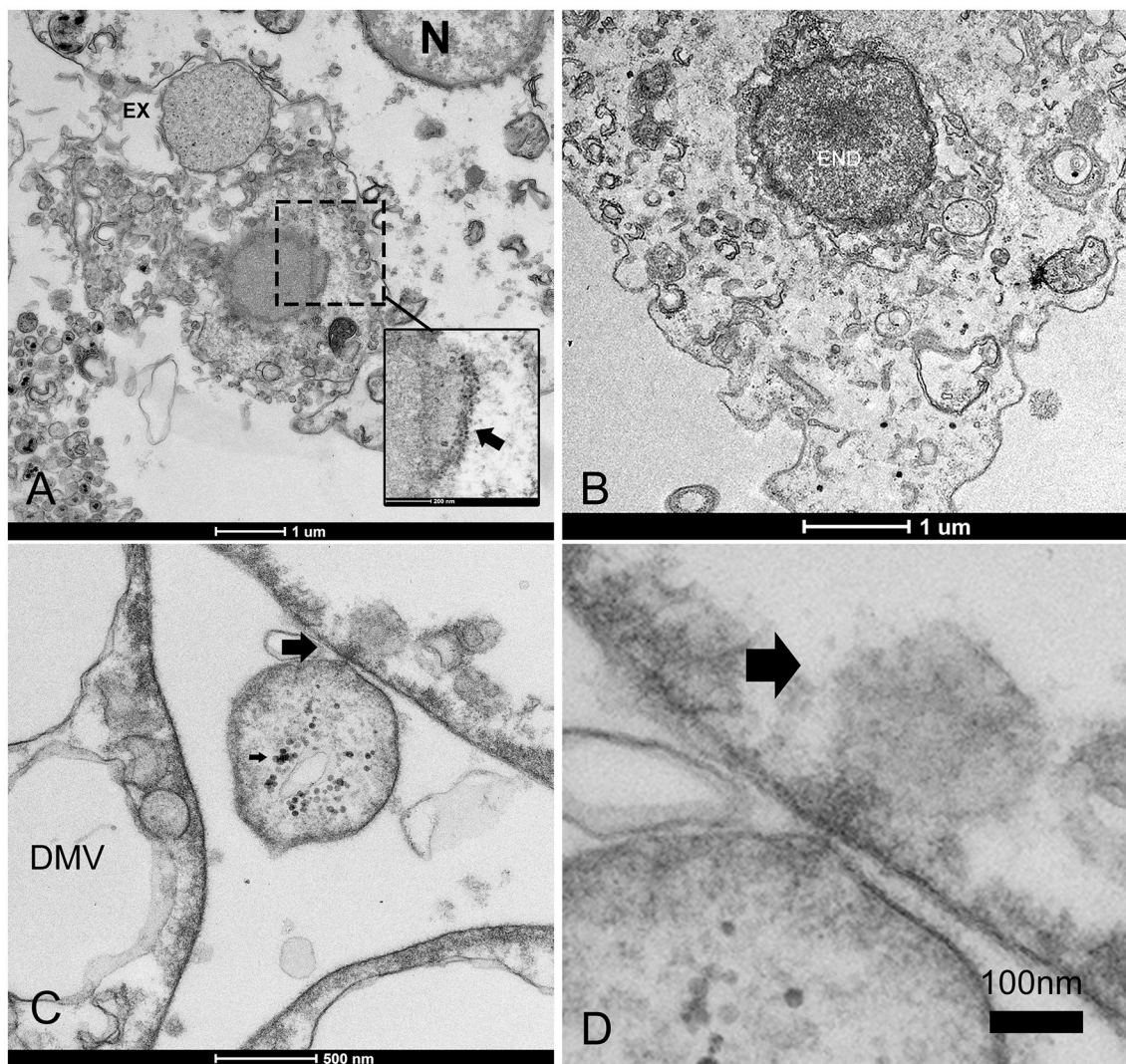


FIGURE 6

Infectious vesicles containing viral particles enter the cells. (A, B) Infectious vesicles containing unassembled viral particles can enter through endocytosis, fusing with the cellular membrane and forming virions (inset, arrow) during the release of exosomes (EXs), which are then transported as late endosomes (ENDs) close to the nucleus (B); (C, D) The vesicle can inject its content into other cells (arrows).

extracellular infective vesicles spreading into the hemolymph, suggesting an active infective phase.

PNPicorF/R designed for the sequence DN9545 did not provide a detectable amplification signal.

### 3.3 Detection of RNA virus in *P. nobilis* hemocytes by quantitative real-time PCR

The quantitative real-time PCR experiments conducted on the cDNA of the *P. nobilis* hemocytes collected at different sampling points in Catalonia were positive for the primer pair PNChetoF/R designed on the reconstructed DN35348\_DN58105 sequence, similar to a *Chaetoceros tenuissimus* RNA virus type II. These results confirm the *in silico* analysis of viral read abundance (Table 5), with Trab8a and XIR2a showing the highest infection level and XIR5 showing a low infection level (Figure 10). With the same primer pair, viral RNA was detected in all other examined samples, presenting variable infection levels. The primer pair

## 4 Discussion

This study reports the discovery of a picornavirus affecting *P. nobilis* hemocytes in Spain and Italy during MMEs (1, 4, 52). Previous studies investigating the etiological agent involved in MMEs showed a complex pattern: disease diagnosis repeatedly confirmed the simultaneous presence of several agents, such as *Haplosporidium pinnae* and *Mycobacterium* spp. (1, 4, 13), *Vibrio mediterranei* (53), and in some cases *Perkinsus* spp., suggesting that a common primary cause, not yet identified, could be linked to these phenomena (4). Based on our observations, this picornavirus could be the underlying cause of these events, as the virus was actively replicating and infecting *P. nobilis* shell immune cells in

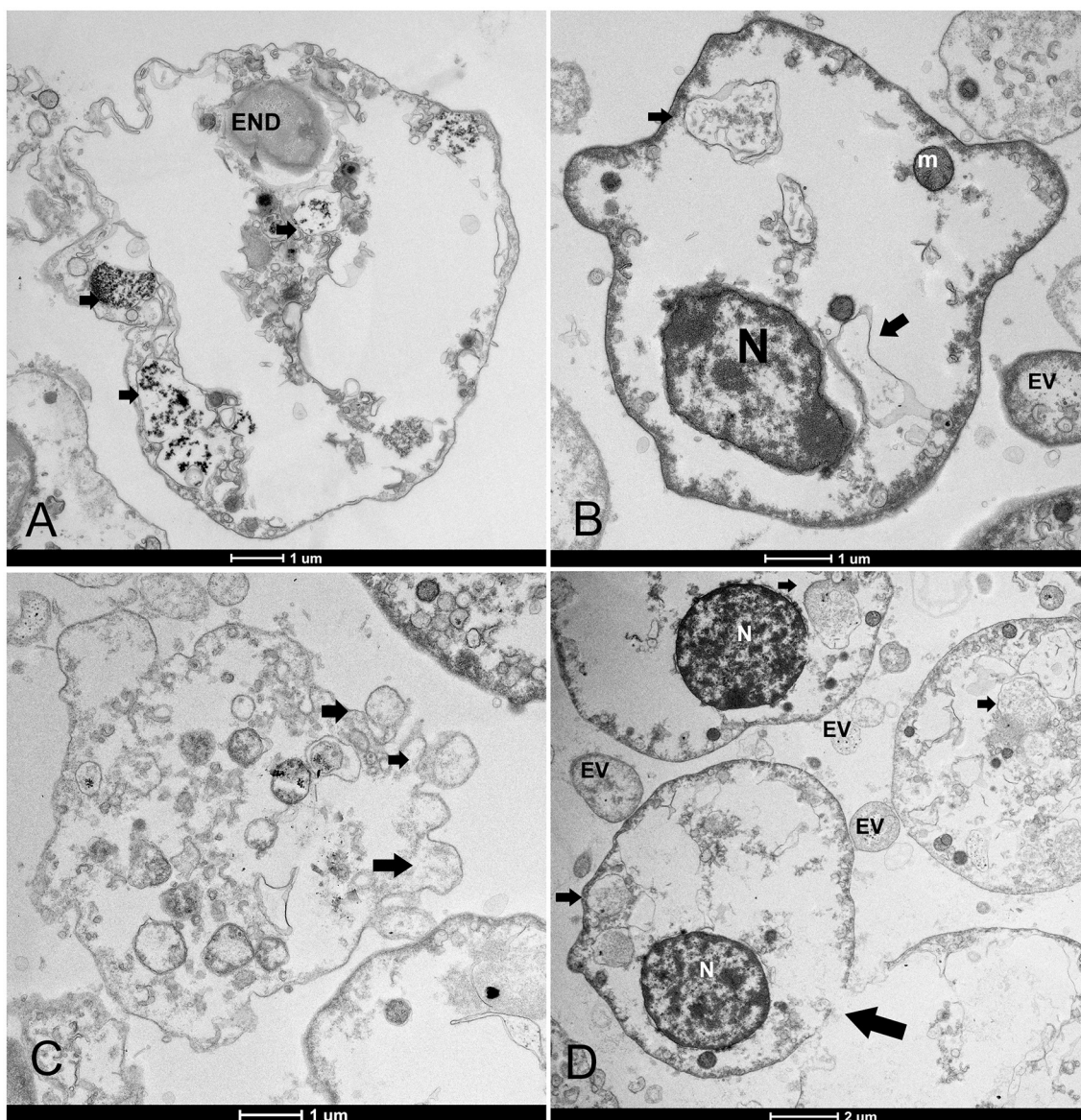


FIGURE 7

Hemocyte cell death. (A, B) Changes mainly include empty cytoplasm with residual vesicles (arrows) or endocytotic vesicles (ENDs) surrounded by extracellular vesicles (EVs); (C) blebbing of the plasma membrane and formation of apoptotic bodies (arrows) and loss of nuclei; (D) membrane rupture (arrows). N, nucleus; m, mitochondria.

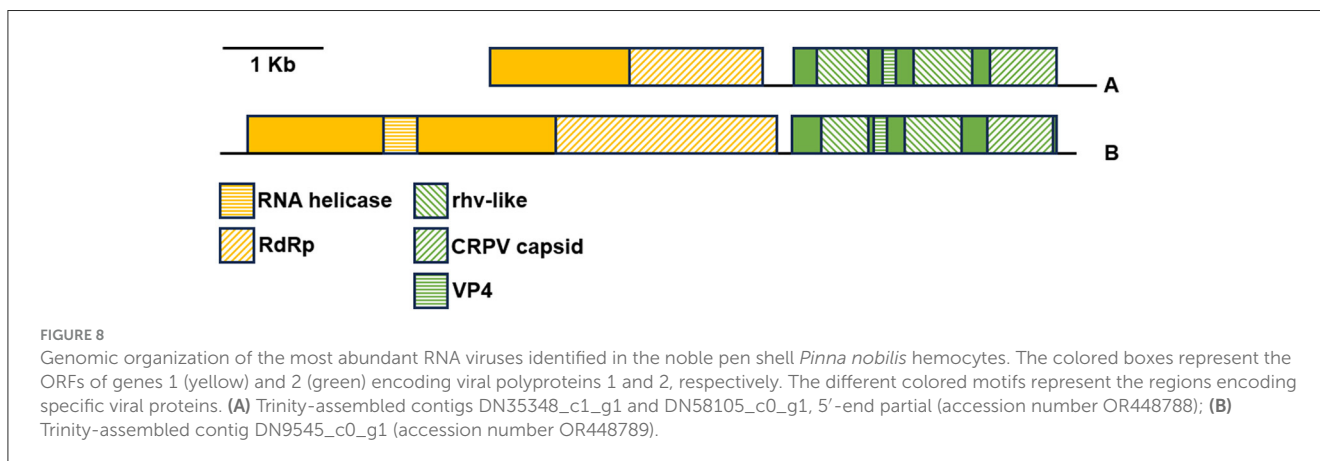
100% of the examined residual populations in Italy and Spain from 2021 to 2023. In fact, the detection of this virus in the same populations over a 2-year period suggests that animals can maintain persistent infections until the disease becomes chronic, weakening them and making them susceptible to opportunistic infections, as also reported in other immunosuppressive viruses (54). This could explain the apparent resistance of the residual individuals who are slowly dying in all areas. The affected animals remain apparently healthy for months to years before the immune system begins to collapse, as reported by many scientists (3, 11, 52).

In this study, the observed picornavirus affecting *P. nobilis* in Italy and Spain used granulocytes and hyalinocytes as vessels for dissemination, replication, and long-term persistence, interfering with hemocyte immune abilities, as observed in

other picornaviruses (55). Multiple known immunoregulatory mechanisms play a role in persistent viral infections, resulting in immunosuppression (56). Immunodeficiency viruses have been reported worldwide in felid, bovine (dairy cattle), and primate (chimpanzee) species and have been observed actively replicating in blood and lymphoid tissues (57). As a result of complete or unsuccessful viral replication, immunodeficiency viruses may functionally lyse or impair immune cells such as lymphocytes, as observed in parvovirus infections of B lymphocytes, in infectious mononucleosis due to Epstein-Barr virus, and in CD4<sup>+</sup> T lymphocytes and macrophages in AIDs caused by HIV lentivirus (58, 59). In other cases, viruses can infect, and damage cells involved in phagocytosis, such as macrophages, as seen in influenza virus and dengue virus infections (60, 61). Similarly, PV can block the

TABLE 5 Assembled contigs classified into the realm *Riboviria* by VirSorter2 and VirBot analysis, the results of their annotation through BLASTX vs. the viral protein database, and read abundance in the different noble pen shell *Pinna nobilis* samples expressed as raw counts.

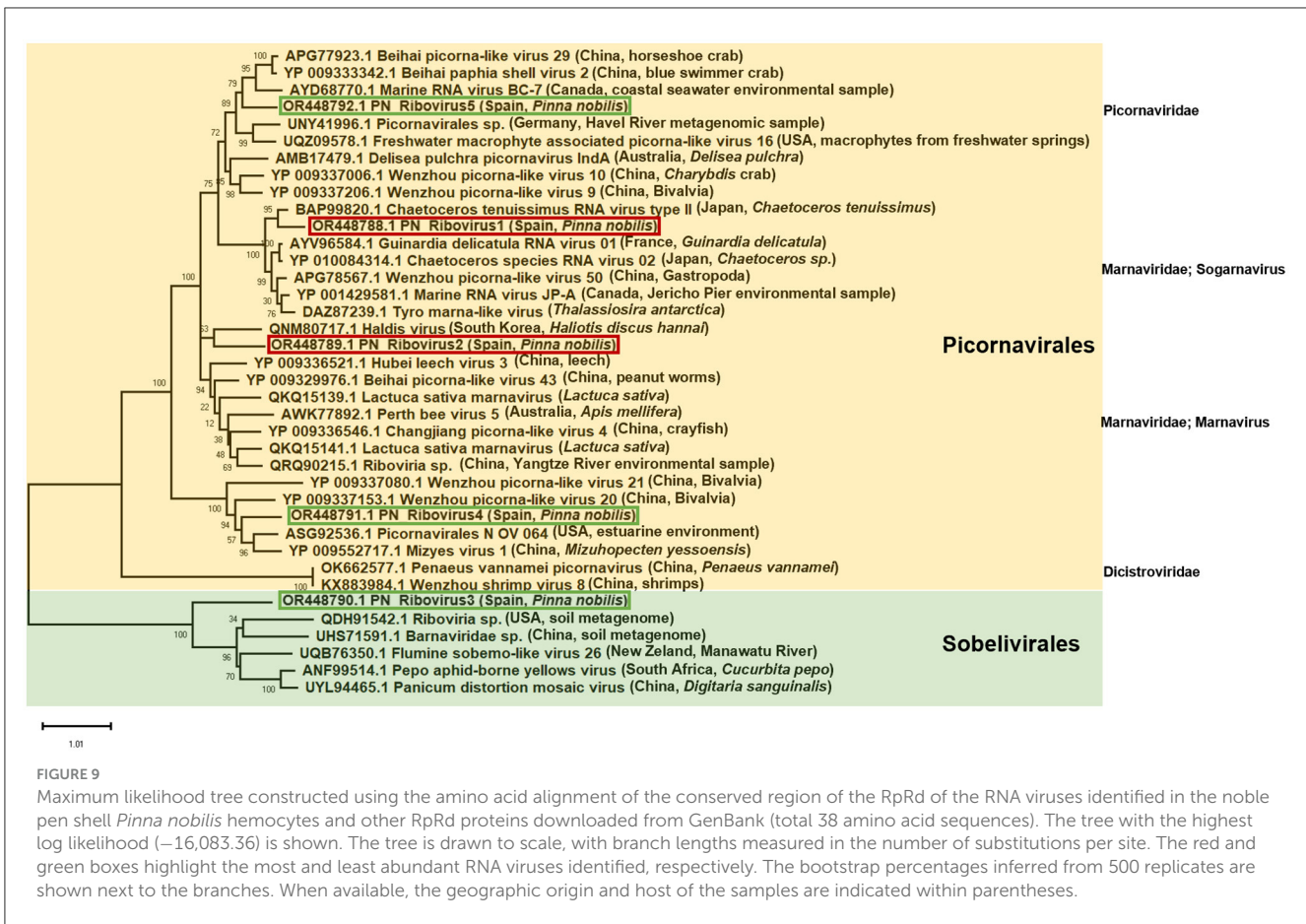
Trinity contig name	Length (nt)	Best BLASTX hit	Bar1	Bar2	Trab8a	Trab8b	XIR2a	XIR5
TRINITY_DN35348_c1_g1	5,210	Predicted structural protein [ <i>Chaetoceros tenuissimus</i> RNA virus type II] BAP99821.1	102	57	6,544	4,113	255	89
TRINITY_DN9545_c0_g1	8,505	Polyprotein [ <i>Picornavirales</i> sp.] UNY42036.1	13	3,755	3,675	4,432	19	11
TRINITY_DN33054_c0_g1	8,876	Putative non-structural protein [ <i>Picornavirales</i> N_OV_064] putative structural protein, partial [ <i>Picornavirales</i> N_OV_064] ASG92536.1	3	364	406	509	2	1
TRINITY_DN33329_c0_g1	5,810	P1–P2 fusion protein [Pepo aphid-borne yellows virus] ANF99514.1	1.05	411.89	345.38	413.98	2.09	0
TRINITY_DN37302_c0_g1	8,567	Polyprotein [marine RNA virus BC-7] AYD68770.1	0	415	386	466	5	0



production of type I interferon (IFN), leading to T-cell depletion, or modulate immune cell apoptosis and autophagy mechanisms (62–64). In bivalves, the primary role of hemocytes is pathogen killing and elimination through phagocytosis, encapsulation, production of cytotoxic molecules and antimicrobial peptides, and secretion of inflammatory cytokines (65–68). A morpho-functional description of *P. nobilis* hemocytes was performed prior to the mortality events in 2015, showing that healthy hemocytes were able to conduct phagocytosis (69). In our study, *P. nobilis* hemocytes from individuals sampled in Spain and Italy displayed damage in mitochondria, ER, and other organelles, which may have affected their regular immune function (70). This is also true considering that a preliminary study performed in *P. nobilis* shell hemocytes from the same areas in 2021–2022 already revealed strong immunodepression, represented by a decreased immune cell response to pathogenic stimuli following an *in vivo* challenge (11).

Immunosuppression is necessary for PVs to use cell components to promote infection (55). PVs have evolved the ability to usurp infected cells' endogenous functions, inducing (endo)membrane rearrangements that are referred to as viral replication organelles (71). Recent work revealed that picornaviruses pack multiple viral particles into a cellular

microvesicle to promote the spread of several heterogeneous virions at a time (72). In this context, the production of EVs and endocytic vesicles plays an important role in the pathogenesis and establishment of viral genome persistence and latency; moreover, viruses that establish chronic infections have been shown to modulate the production and content of more infectious EVs, increasing their infective potential (73). Animals maintained in captivity in this study displayed a high number of infective vesicles and dead cells, which was also related to hemocytopenia. Persistent PV infection can induce lymphopenia in humans and animals, such as cows, cats, and birds, as a direct result of viral infection or indirectly through cytokine induction (55, 74). Along with other diagnostic indices, decreased THC is a critical condition in the progression of an infection or a disease in invertebrates (75). Hemocytopenia has been observed during chronic viral infections, such as abalone ganglioneuritis (76), and during bacterial and parasitic diseases in other mollusk species (77, 78). Typically, persistent infections bring a relatively small pool of hemocytes into the hemolymph sinuses and perivisceral beds, and such sequestration into tissues may lead to a dramatic decrease in hemocyte numbers (79). Before the observation of mass mortality in the Mediterranean, Matozzo et al. (69) reported a higher number



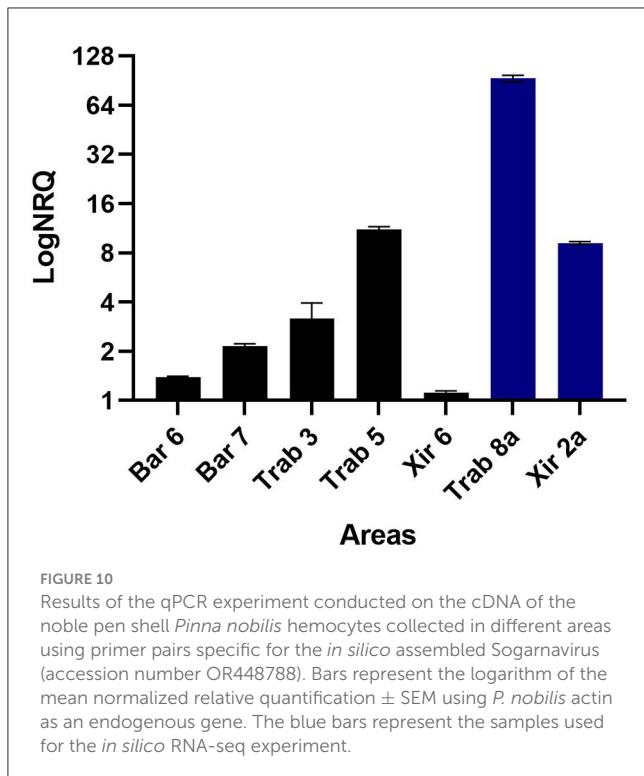
of circulating hemocytes ( $5 \times 10^5$  cells) in comparison to that in the current Spanish wild and captive populations. Based on our results, this finding could indicate an over-time immune cell decrease due to infection and a worsened situation for animals maintained in tanks. Apart from hemocyte sequestration into infected tissues, such hemocytopenia is also possibly caused by apoptosis due to hemocyte infection (80). This host-initiated process of programmed cell death is essential for normal cell turnover and functions as an antiviral mechanism to limit the spread of a virus (81, 82).

In the present study, we were able to assemble different *Riboviria* sequences of the orders *Picornavirales* and *Sobelivirales*, with NGS Illumina sequencing obtaining nearly five different genomes accompanied by phylogenetic analysis. Our findings support previous observations that bivalve and other invertebrate viromes harbor a broad diversity of viruses of the order *Picornavirales* (25, 83), matching the ultrastructural features of hemocyte PV infection. Picornaviruses are components of the virome associated with filter-feeding organisms under normal physiological conditions, as reported in metatranscriptomic studies in the absence of detectable disease (84). Among the five assembled *Riboviria*, the two most abundant sequences are clustered with the *Picornavirales* group within the family *Marnaviridae*, which comprises small non-enveloped viruses that infect various photosynthetic marine protists (85) and have also been reported in diatom populations (86). The most abundant reads placed

the hemocyte PV close to a virus isolated in the marine diatom *Chaetoceros tenuissimus*, named *C. tenuissimus* RNA virus type II (86), belonging to the genus *Sogarnavirus*, while the second most abundant PV was identified as *Picornavirus*, belonging to the genus *Marnavirus*.

Microalgal cells infected by *Marnaviridae*, genus *Sogarnavirus*, can display extensive cytopathic effects with ultrastructural changes, including swelling of the endoplasmic reticulum, vacuolation, and disintegration of the cytoplasm (86, 87), as reported in our study. To the best of our knowledge, this is the first report of a sogarnavirus affecting an animal species. To confirm the NGS analysis, qPCR was performed to amplify the most represented *Sogarnavirus*. The primer pairs designed on the sequence of the *P. nobilis* picornavirus similar to the *C. tenuissimus* RNA virus type II were positive in the analyzed samples, while no amplification was obtained with the other primer pairs. These results may not be conclusive and need to be confirmed with other analyses.

In this study, both apparently healthy and sick animals showed ultrastructural features of viral infection. In confined waters across Mediterranean regions, such as lagoons, MMEs started later (52). For instance, in Venice Lagoon, mortality episodes began in 2020, which is after the *P. nobilis* populations started dying off of the Ebro Delta, which started in 2018 (4). The viral infection could have originated first in Spanish waters, years before mortalities became evident, subsequently reaching other areas, until animals presented



an acquired immunodeficiency (i.e., low count of hemocytes), as occurs with other immunodeficiency viruses. The disease, made up of periods of remission followed by disease progression over time, ends up gradually weakening the populations that start to display symptoms, leading to population decline. These individuals are exposed to a wide variety of bacterial and parasitic opportunistic infections, resulting in an unfavorable situation. In the Venice Lagoon, in the area where animals appeared apparently healthy in May 2023, remarkable mortality was observed 2 months later. In the four analyzed individuals, all immune cells presented actively replicating virus. This means that infection can be subclinical until very late in the process, which is when an opportunistic pathogen is more likely to take advantage of the situation.

As previously reported, recent findings suggest a more complex scenario than the one originally proposed in the first descriptions of *P. nobilis* MMEs (1, 4, 13). Diseases with complex etiology are influenced by various interacting drivers and frequently remain difficult to characterize. Indeed, this viral disease represents an epidemiological threat of unknown proportions for marine animal populations. Further studies are needed to determine the ecological importance of PV as an agent affecting the dynamics of *P. nobilis* MMEs in the analyzed areas and in other natural environments.

## 5 Conclusion

Few viruses, mainly those belonging to the families of *Alloherpesviridae* and *Iridoviridae*, have been associated with disease outbreaks and mortality in bivalves. Nevertheless, picornavirus-like particles have also been reported during disease outcomes (88–90). Here, we report the first description of an

immunodeficiency virus in bivalves affecting *P. nobilis* hemocytes. Immune defense is a key determinant of fitness, underlying the capacity of animals to resist or tolerate potential infections. Immune function is not static and can be suppressed, depressed, or stimulated by exposure to environmental abiotic factors, food availability, and pathogens. Alteration of this response can directly affect population dynamics and survival. Recently, the emergence and spread of new and existing pathogens have posed a significant risk not only to human life and animal health but also to the conservation of wildlife. Future studies are needed to establish a clear and significant correlation between the genome of the picornaviruses assembled in *P. nobilis* hemocytes and the *P. nobilis* MMEs. First, the full length of the partial PV sequence assembled *in vitro* should be obtained using a 5'RACE approach. Second, viral isolation and cultivation attempts are needed to define virus characteristics. Finally, a fast and reliable diagnostic test (e.g., based on qPCR) should be developed to rapidly check the infection level of the surviving *P. nobilis* populations in other geographic areas. Virus presence should also be evaluated in the environment (water, plankton, sediments) and surrounding animals, which could be potential virus reservoirs.

## Data availability statement

The original contributions presented in the study are publicly available. This data can be found here: <https://www.ncbi.nlm.nih.gov/bioproject>; PRJNA999583.

## Ethics statement

The animal study was approved by MATTM Ministero dell'ambiente e della sicurezza energetica. The study was conducted in accordance with the local legislation and institutional requirements.

## Author contributions

FC: Conceptualization, Data curation, Formal analysis, Funding acquisition, Investigation, Methodology, Supervision, Validation, Writing—original draft, Writing—review & editing. PP: Investigation, Resources, Writing—review & editing. GD: Writing—review & editing. DP: Writing—review & editing. GV: Methodology, Writing—review & editing. JG-M: Resources, Writing—review & editing. JT-M: Resources, Writing—review & editing. EC: Resources, Writing—review & editing. FG-C: Resources, Writing—review & editing. MS: Writing—review & editing. SA: Data curation, Formal analysis, Software, Supervision, Writing—original draft, Writing—review & editing.

## Funding

The author(s) declare financial support was received for the research, authorship, and/or publication of this article. The research was partially supported by the EU LIFE Programme Project Protection and restoration of *Pinna nobilis* populations as

a response to the catastrophic pandemic started in 2016 (LIFE PINNARCA) (grant number LIFE20 NAT/ES/001265).

## Acknowledgments

The authors thank Dr. Sergio Sorbo of the CeSMA, Section of Microscopy LaMMEC, University of Naples Federico II, and Dr. Antonella Giarra, Chemistry Department of the University of Naples Federico II, for technical support in electron microscopy. The authors also thank José Luis Costa and David Mateu Vilella (IRTA) and Roberto Vianello with Andrea Sabino (CNR-ISMAR) for technical assistance during fieldwork sampling in Catalonia and Venice, respectively.

## Conflict of interest

The authors declare that the research was conducted in the absence of any commercial or financial relationships that could be construed as a potential conflict of interest.

The reviewer IG declared a past co-authorship with the authors FC, DP, GD, JT-M, and JG-M to the handling editor.

## References

- Carella F, Aceto S, Pollaro F, Miccio A, Iaria C, Carrasco N, et al. A mycobacterial disease is associated with the silent mass mortality of the pen shell *Pinna nobilis* along the Tyrrhenian coastline of Italy. *Sci Rep.* (2019) 9:1–12. doi: 10.1038/s41598-018-37217-y
- Kersting D, Benabdi M, Čižmek H, Grau A, Jimenez C, Katsanevakis S, et al. *Pinna nobilis* in the Greek seas (NE Mediterranean): on the brink of extinction? *The IUCN Red List of Threatened Species.* (2019). 24 p. Available online at: <https://www.iucnredlist.org/species/160075998/160081499>
- Zotou M, Gkrantounis P, Karadimou E, Tsirintanis K, Sini M, Poursanidis D, et al. *Pinna nobilis* in the Greek seas (NE Mediterranean): on the brink of extinction? *Mediterr Mar Sci.* (2020) 21:575–91. doi: 10.12681/mms.23777
- Carella F, Antuofermo E, Farina S, Salati F, Mandas D, Prado P, et al. In the wake of the ongoing mass mortality events: co-occurrence of *Mycobacterium*, *Haplosporidium* and other pathogens in *Pinna nobilis* collected in Italy and Spain (Mediterranean Sea). *Front Mar Sci.* (2020) 7:48. doi: 10.3389/fmars.2020.00048
- Lattos A, Feidantsis K, Georgoulis I, Giantsis IA, Karagiannis D, Theodorou JA, et al. Pathophysiological responses of *Pinna nobilis* individuals enlightens the etiology of mass mortality situation in the mediterranean populations. *Cells.* (2021) 22:2838. doi: 10.3390/cells10112838
- Katsanevakis S. The cryptogenic parasite *Haplosporidium pinnae* invades the Aegean Sea and causes the collapse of *Pinna nobilis* populations. *Aquat Invasions.* (2019) 14:150–64. doi: 10.3391/ai.2019.14.2.01
- Vázquez-Luis M, Alvarez E, Barrajon A, García-March JR, Grau A, Hendricks IE, et al. S.O.S. *Pinna nobilis*: a mass mortality event in western Mediterranean Sea. *Front Mar Sci.* (2017) 4:109. doi: 10.3389/fmars.2017.00220
- Katsanevakis S, Carella F, Çinar ME, Čižmek H, Jimenez C, Kersting DK, et al. The fan mussel *Pinna nobilis* on the brink of extinction in the Mediterranean. In: Dellasala DA, Goldstein MI, editors. *Imperiled: the Encyclopedia of Conservation.* Oxford: Elsevier (2022).
- Darriba S. First haplosporidan parasite reported infecting a member of the Superfamily Pinnoidae (*Pinna nobilis*) during a mortality event in Alicante (Spain, Western Mediterranean). *J Invertebr Pathol.* (2017) 148:14–9. doi: 10.1016/j.jip.2017.05.006
- Catanese G, Grau A, Valencia JM, Garcia-March JR, Vazquez-Luis M, Alvarez E, et al. *Haplosporidium pinnae* sp. nov, a haplosporidan parasite associated with mass mortalities of the fan mussel, *Pinna nobilis*, in the Western Mediterranean Sea. *J Invertebr Pathol.* (2018) 157:9–24. doi: 10.1016/j.jip.2018.07.006
- Carella F, Prado P, García-March JR, Medialdea JT, Cortés Melendreras E, Giménez Casalduero E, et al. *Phagocytosis Based Assay for an In Vitro Assessment of*

## Publisher's note

All claims expressed in this article are solely those of the authors and do not necessarily represent those of their affiliated organizations, or those of the publisher, the editors and the reviewers. Any product that may be evaluated in this article, or claim that may be made by its manufacturer, is not guaranteed or endorsed by the publisher.

## Supplementary material

The Supplementary Material for this article can be found online at: <https://www.frontiersin.org/articles/10.3389/fvets.2023.1273521/full#supplementary-material>

### SUPPLEMENTARY FIGURE 1

Genomic organization of the less abundant RNA viruses identified in the noble pen shell *Pinna nobilis* hemocytes. The colored boxes represent the ORFs of genes 1 (yellow) and 2 (green) encoding viral polyproteins 1 and 2, respectively. (A) Trinity-assembled contig DN33329\_c0\_g1 (accession number OR448790); (B) Trinity-assembled contig DN33054\_c0\_g1 (accession number OR448791); (C) Trinity-assembled contig DN37302\_c0\_g1 (accession number OR448792).

*Immunocompetence of the Pen Shell P. nobilis During Mass Mortality Events.* Aberdeen: EAAP European Association of Fish pathologist Congress (2023).

- Grau A, Villalba A, Navas JI, Hansjosten B, Valencia JM, García-March JR, et al. Wide-geographic and long-term analysis of the role of pathogens in the decline of *Pinna nobilis* to critically endangered species. *Front Mar Sci.* (2022) 9:303. doi: 10.3389/fmars.2022.666640
- Carella F, Palić D, Šarić T, Župan I, Gorgoglione B, Prado P, et al. Multi-pathogen infections and multifactorial pathogenesis involved in noble pen shell (*Pinna nobilis*) mass mortality events: background and current pathologic approaches. *Vet Pathol.* (2023) 60:560–77. doi: 10.1177/03009858231186737
- Le Gall O, Christian P, Fauquet CM, King AMQ, Knowles NJ, Nakashima N, et al. *Picornavirales*, a proposed order of positive-sense single-stranded RNA viruses with a pseudo-T = 3 virion architecture. *Arch Virol.* (2008) 153:715. doi: 10.1007/s00705-008-0041-x
- Wang-Shick R. Chapter 11, picornavirus. In: *Molecular Virology of Human Pathogenic Viruses.* (2017). p. 153–64.
- Stanway G. Structure, function and evolution of picornaviruses. *J Gen Virol.* (1990) 71(Pt 11):2483–501. doi: 10.1099/0022-1317-71-11-2483
- Gustavsen JA, Winget DM, Tian X, Suttle CA. High temporal and spatial diversity in marine RNA viruses implies that they have an important role in mortality and structuring plankton communities. *Front Microbiol.* (2014) 5:703. doi: 10.3389/fmicb.2014.00703
- Whitton JL, Cornell CT, Feuer R. Host and virus determinants of picornavirus pathogenesis and tropism. *Nat Rev Microbiol.* (2005) 3:765–76.
- Cifuentes JO, Moratorio G. Evolutionary and structural overview of human picornavirus capsid antibody evasion. *Front Cell Infect Microbiol.* (2019) 9:283. doi: 10.3389/fcimb.2019.00283
- Zell R, Delwart E, Gorbalenya E, Hovi T. ICTV virus taxonomy profile. *Picornaviridae.* (2017) 98:2421–2. doi: 10.1099/jgv.0.000911
- Baltimore D. Expression of animal virus genomes. *Bacteriol Rev.* (1971) 35:235–41. doi: 10.1128/br.35.3.235-241.1971
- Arcier J-M, Herman F, Lightner DV, Redman RM, Mari J, Bonami JR. A viral disease associated with mortalities in hatchery-reared postlarvae of the giant freshwater prawn *Macrobrachium rosenbergii*. *DAO.* (1999) 38:177–81. doi: 10.3354/dao038177
- Tang KFJ, Lightner DV. Phylogenetic analysis of Taura syndrome virus isolates collected between 1993 and 2004 and virulence comparison between

- two isolates representing different genetic variants. *Virus Res.* (2005) 112:69–76. doi: 10.1016/j.virusres.2005.03.023
24. Kapoor A, Victoria J, Simmonds P, Wang C, Shafer R, Nims W, et al. A highly divergent picornavirus in a marine mammal. *iVirol.* (2008) 82:311–20. doi: 10.1128/JVI.01240-07
25. Shi M, Lin XD, Tian JH, Chen LJ, Chen X, Li CX, et al. Redefining the invertebrate RNA virosphere. *Nature.* (2016) 540:539–43. doi: 10.1038/nature20167
26. Kim J-O, Lee JK, Seo YB, Lim H-K, Kim G-D. Genome sequences of a novel picorna-like virus from Pacific abalone (*Haliotis discus hannai*) in South Korea. *Genome Announc.* (2017) 5:e00484–17. doi: 10.1128/genomeA.00484-17
27. Liu S, Xu T, Wang C, Jia T, Zhang Q. A novel picornavirus discovered in white leg shrimp *Penaeus vannamei*. *Viruses.* (2021) 13:2381. doi: 10.3390/v13122381
28. Belov GA, Nair V, Hansen BT, Hoyt FH, Fischer ER, Ehrenfeld E. Complex dynamic development of poliovirus membranous replication complexes. *J Virol.* (2012) 86:302–12. doi: 10.1128/JVI.05937-11
29. Harak C, Lohmann V. Ultrastructure of the replication sites of positive-strand RNA viruses. *Virology.* (2015) 479–80:418–33. doi: 10.1016/j.virol.2015.02.029
30. Dales S, Eggers HJ, Tamm I, Palade GE. Electron microscopic study of the formation of poliovirus. *Virology.* (1965) 26:379–89. doi: 10.1016/0042-6822(65)90001-2
31. Hsu N-Y, Ihlytska O, Belov G, Santiana M, Chen YH, Takvorian PM, et al. Viral reorganization of the secretory pathway generates distinct organelles for RNA replication. *Cell.* (2010) 141:799–811. doi: 10.1016/j.cell.2010.03.050
32. Suhly DA, Giddings TH Jr, Kirkegaard K. Remodeling the endoplasmic reticulum by poliovirus infection and by individual viral proteins: an autophagy-like origin for virus-induced vesicles. *J Virol.* (2000) 74:8953–65. doi: 10.1128/JVI.74.19.8953-8965.2000
33. Cottam E, Pierini R, Roberts R, Wileman T. Origins of membrane vesicles generated during replication of positive-strand RNA viruses. *Fut. Virol.* (2009) 4:473–85. doi: 10.2217/fvl.09.26
34. Yang JE, Rossignol ED, Chang D, Zaia J, Forrester I, Raja K, et al. Complexity and ultrastructure of infectious extracellular vesicles from cells infected by nonenveloped virus. *Sci Rep.* (2020) 10:1–18. doi: 10.1038/s41598-020-64531-1
35. Welsch S, Müller B, Kräusslich H-G. More than one door - Budding of enveloped viruses through cellular membranes. *FEBS Lett.* (2007) 581:2089–97. doi: 10.1016/j.febslet.2007.03.060
36. den Boon JA, Diaz A, Ahlquist P. Cytoplasmic viral replication complexes. *Cell Host Microbe.* (2010) 8:77–85. doi: 10.1016/j.chom.2010.06.010
37. Prado P, Grau A, Catanese G, Cabanes P, Carella F, Fernández-Tejedor M, et al. *Pinna nobilis* in suboptimal environments are more tolerant to disease but more vulnerable to severe weather phenomena. *Mar Environ Res.* (2021) 163:105220. doi: 10.1016/j.marenvres.2020.105220
38. Gimenez-Casaldueiro F, Martínez-Fernández J. El colapso del mar menor: historia de una joya ecológica maltratada. *Metode Rev difusión la Investig.* (2020) 106:22–9.
39. Cortés-Melendreras E, Gomariz-Castillo F, Alonso-Sarría F, Martín FJG, Murcia J, Canales-Cáceres R, et al. The relict population of *Pinna nobilis* in the Mar Menor is facing an uncertain future. *Mar Pollut Bull.* (2022) 185:114376. doi: 10.1016/j.marpolbul.2022.114376
40. Tagliapietra D, Zanon V, Frangipane G, Umgiesser G, Sigovini M. Physiographic zoning of the Venetian lagoon. In: Camprostrini P, editor. *Scientific Research and Safeguarding of Venice, vol. VII - 2007-2010*. Venezia: CORILA (2009). p. 161–4.
41. Bolger AM, Lohse M, Usadel B. Trimmomatic: a flexible trimmer for illumina sequence data. *Bioinformatics.* (2014) 30:2114–20. doi: 10.1093/bioinformatics/btu170
42. Langmead B, Salzberg S. Fast gapped-read alignment with Bowtie 2. *Nat Methods.* (2012) 9:357–9. doi: 10.1038/nmeth.1923
43. Danecek P, Bonfield JK, Liddle J, Marshall J, Ohan V, Pollard MO, et al. Twelve years of SAMtools and BCFtools. *GigaScience.* (2021) 10:giab008. doi: 10.1093/gigascience/giab008
44. Grabherr MG, Haas BJ, Yassour M, Levin JZ, Thompson DA, Amit I, et al. Full-length transcriptome assembly from RNA-seq data without a reference genome. *Nat Biotechnol.* (2011) 29:644–52. doi: 10.1038/nbt.1883
45. Li B, Dewey CN. RSEM: accurate transcript quantification from RNA-Seq data with or without a reference genome. *BMC Bioinform.* (2012) 12:323. doi: 10.1186/1471-2105-12-323
46. Guo J, Bolduc B, Zayed AA, Varsani A, Dominguez-Huerta G, Delmont TO, et al. VirSorter2: a multi-classifier, expert-guided approach to detect diverse DNA and RNA viruses. *Microbiome.* (2021) 9:37. doi: 10.1186/s40168-020-00990-y
47. Chen G, Tang X, Shi M, Sun Y. VirBot: an RNA viral contig detector for metagenomic data. *Bioinformatics.* (2023) 39:btad093. doi: 10.1093/bioinformatics/btad093
48. Kumar S, Stecher G, Li M, Knyaz C, Tamura K. MEGA X: molecular evolutionary genetics analysis across computing platforms. *Mol Biol Evol.* (2018) 35:1547–9. doi: 10.1093/molbev/msy096
49. Lattos A, Papadopoulos DK, Giantsis IA, Feidantsis K, Georgoulis I, Karagiannis D, et al. Investigation of the highly endangered *Pinna nobilis* mass mortalities: Seasonal and temperature patterns of health status, antioxidant and heat stress responses. *Mar Environ Res.* (2023) 188:105977. doi: 10.1016/j.marenvres.2023.105977
50. Huan P, Wang H, Liu B. Assessment of housekeeping genes as internal references in quantitative expression analysis during early development of oyster. *Gene Genet Syst.* (2016) 91:257–65. doi: 10.1266/ggs.16-00007
51. Srisala J, Thaiue D, Saganrut P, Taengchaiyaphum, Flegel TW, Sritunyalucksana K. Wenzhou shrimp virus 8 (WzSV8) detection by unique inclusions in shrimp hepatopancreatic E-cells and by RT-PCR. *Aquaculture.* (2023) 572:739483. doi: 10.1016/j.aquaculture.2023.739483
52. Šarić T, Župan I, Aceto S, Villari G, Palic D, De Vico G, et al. Epidemiology of noble pen shell (*Pinna nobilis* L. 1758) mass mortality events in adriatic sea is characterised with rapid spreading and acute disease progression. *Pathogens.* (2020) 9:1–21. doi: 10.3390/pathogens9100776
53. Prado P, Carrasco N, Catanese G, Grau A, Cabanes P, Carella F, et al. Presence of *Vibrio mediterranei* associated to major mortality in stabled individuals of *Pinna nobilis* L. *Aquaculture.* (2020) 519:734899. doi: 10.1016/j.aquaculture.2019.734899
54. English RV, Nelson P, Johnson CM, Nasisse M, Tompkins WA, Tompkins MB. Development of clinical disease in cats experimentally infected with feline immunodeficiency virus. *J Infect Dis.* (1994) 170:543–52. doi: 10.1093/infdis/170.3.543
55. Cusick MF, Libbey JE, Fujinami RS. Picornavirus infection leading to immunosuppression. *Fut Virol.* (2014) 9:475–82. doi: 10.2217/fvl.14.26
56. Oldstone MB. Anatomy of viral persistence. *PLoS Pathog.* (2009) 5:e1000523. doi: 10.1371/journal.ppat.1000523
57. Tizard I. *Secondary Immunodeficiencies*. The Merck Veterinary Manual (2019). Available online at: <https://www.merckvetmanual.com/immune-system/immunologic-diseases/secondary-immunodeficiencies#v3277197> (accessed July 22, 2023).
58. Ackley CD, Yamamoto JK, Levy N, Pedersen NC, Cooper MD. Immunologic abnormalities in pathogen-free cats experimentally infected with feline immunodeficiency virus. *J Virol.* (1990) 64:5652–5. doi: 10.1128/jvi.64.11.5652-5655.1990
59. Brown MA, Munkhtsog B, Troyer JL, Ross S, Sellers R, Fine AE, et al. Feline immunodeficiency virus (FIV) in wild Pallas's cats. *Vet Immunol Immunopathol.* (2010) 134:90–5. doi: 10.1016/j.vetimm.2009.10.014
60. Egberink H, Horzinek MC. Animal immunodeficiency viruses. *Vet Microbiol.* (1992) 33:311–31. doi: 10.1016/0378-1135(92)90059-3
61. VandeWoude S, Apetrei C. Going wild: lessons from naturally occurring T-lymphotropic lentiviruses. *Clin Microbiol Rev.* (2006) 19:728–62. doi: 10.1128/CMR.00009-06
62. Lei X, Sun Z, Liu X, Jin Q, He B, Wang J. Cleavage of the adaptor protein TRIF by enterovirus 71 3C inhibits antiviral responses mediated by Toll-like receptor 3. *J Virol.* (2011) 85:8811–8. doi: 10.1128/JVI.00447-11
63. Lee YP, Wang YF, Wang JR, Huang SW, Yu CK. Enterovirus 71 blocks selectively type I interferon production through the 3C viral protein in mice. *J Med Virol.* (2012) 84:1779–89. doi: 10.1002/jmv.23377
64. Son KN, Liang Z, Lipton HL. Mutation of the Theiler's virus leader protein zinc-finger domain impairs apoptotic activity in murine macrophages. *Virus Res.* (2013) 177:222–5. doi: 10.1016/j.virusres.2013.09.001
65. de la Ballina NR, Maresca F, Cao A, Villalba A. Bivalve haemocyte subpopulations: a review. *Front Immunol.* (2022) 13:826255. doi: 10.3389/fimmu.2022.826255
66. Song L, Wang L, Qiu L, Zhang H. Bivalve immunity. *Adv Exp Med Biol.* (2010) 708:44–65. doi: 10.1007/978-1-4419-8059-5\_3
67. Cheng TC. Bivalves. In: Ratcliffe NA, Rowley AF, editors. *Invertebrate Blood Cells*. London: Academic Press (1981). p. 233–300.
68. Nakayama K, Nomoto AM, Nishijima M, Maruyama T. Morphological and functional characterization of hemocytes in the giant clam *Tridacna crocea*. *J Invertebr Pathol.* (1997) 69:105e111. doi: 10.1006/jipa.1996.4626
69. Matozzo V, Pagano M, Spinelli A, Caicci F, Faggio C. *Pinna nobilis*: a big bivalve with big haemocytes? *Fish Shellfish Immunol.* (2016) 55:529–34. doi: 10.1016/j.fsi.2016.06.039
70. Pugliese A, Vidotto V, Beltramo T, Torre D. Phagocytic activity in human immunodeficiency virus type 1 infection. *Clin Diagn Lab Immunol.* (2005) 889–95. doi: 10.1128/CDLI.12.8.889-895.2005
71. Meckes DG Jr, Raab-Traub N. Microvesicles and viral infection. *J Virol.* (2011) 85:12844–54. doi: 10.1128/JVI.05853-11
72. Chen YH, Du W, Hagemeyer MC, Takvorian PM, Pau C, Cali A, et al. Phosphatidylserine vesicles enable efficient en bloc transmission of enteroviruses. *Cell.* (2015) 160:619–30. doi: 10.1016/j.cell.2015.01.032
73. Amari L, Germain M. Mitochondrial extracellular vesicles, origins and roles. *Front Mol Neurosci.* (2021) 14:767219. doi: 10.3389/fnmol.2021.767219

74. Geoghegan JL, Duchêne S, Holmes EC. Comparative analysis estimates the relative frequencies of co- divergence and cross- species transmission within viral families. *PLoS Pathog.* (2017) 13:e1006215. doi: 10.1371/journal.ppat.1006215
75. Cheng W, Juang F-M, Chen J-C. The immune response of Taiwan abalone *Haliotis diversicolor supertexta* and its susceptibility to *Vibrio parahaemolyticus* at different salinity levels. *Fish Shellfish Immun.* (2004) 16:295–306. doi: 10.1016/S1050-4648(03)00111-6
76. Hooper C, Hardy-Smith B, Handler J. Ganglioneuritis causing high mortalities in farmed Australian abalone (*Haliotis laevis* and *Haliotis rubra*). *Aust Vet J.* (2007) 85:188–93. doi: 10.1111/j.1751-0813.2007.00155.x
77. Shields JD, Perkins FO. *Parasitological Examination of Wasting Disease in Black Abalone, Haliotis cracherodii: Final Report.* Virginia Institute of Marine Science, William & Mary (1997). Available online at: <https://scholarworks.wm.edu/reports/2760>
78. Handler J, Leonart M, Powell M. *Development of an Integrated Management Program for the Control of Spionid Mudworms in Cultured Abalone.* Canberra, ACT: FRDC Project No 98/307 Fisheries Research and Development Corporation (2004).
79. Hooper C, Slocombe R, Day R, Crawford S. Leucopenia associated with abalone viral ganglioneuritis. *Aust Vet J.* (2012) 90:24–8. doi: 10.1111/j.1751-0813.2011.00877.x
80. Sun D, Wen X, Wang M, Mao S, Cheng A, Yang X, et al. Apoptosis and Autophagy in Picornavirus Infection. *Front Microbiol.* (2019) 10:2032. doi: 10.3389/fmicb.2019.02032
81. Belov GA, Romanova LI, Tolskaya EA, Kolesnikova MS, Lazebnik YA, Agol VI. The major apoptotic pathway activated and suppressed by poliovirus. *J Virol.* (2003) 77:45–56. doi: 10.1128/JVI.77.1.45-56.2003
82. Croft SN, Walker EJ, Ghildyal R. Picornaviruses and apoptosis: subversion of cell death. *Mbio.* (2017) 8:e01009–17. doi: 10.1128/mBio.01009-17
83. Zhou D, Liu S, Guo G, He X, Xing C, Miao Q, et al. Virome analysis of normal and growth retardation disease-affected *Macrobrachium rosenbergii*. *Microbiol Spectr.* (2022) 10:e0146222. doi: 10.1128/spectrum.01462-22
84. Moreira R, Balseiro P, Planas JV, Fuste B, Beltran S, Novoa B, et al. Transcriptomics of in vitro immune-stimulated hemocytes from the Manila clam *Ruditapes philippinarum* using high-throughput sequencing. *PLoS ONE.* (2012) 7:e35009. doi: 10.1371/journal.pone.0035009
85. Sadeghi M, Tomaru Y, Ahola T. RNA viruses in aquatic unicellular eukaryotes. *Viruses.* (2021) 25:362. doi: 10.3390/v13030362
86. Shirai Y, Tomaru Y, Takao Y, Suzuki H, Nagumo T, Nagasaki K. Isolation and characterization of a single-stranded RNA virus infecting the marine planktonic diatom *Chaetoceros tenuissimus* meunier appl. *Environ Microbiol.* (2008) 74:4022–7. doi: 10.1128/AEM.00509-08
87. Nagasaki K, Tomaru Y, Katanozaka N, Shirai Y, Nishida K, Itakura S, et al. Isolation and characterization of a novel single-stranded RNA virus infecting the bloom-forming diatom *Rhizosolenia setigera*. *Appl Environ Microbiol.* (2004) 70:704–11. doi: 10.1128/AEM.70.2.704-711.2004
88. Carballal MJ, Villalba A, Iglesias D, Hine PM. Virus-like particles associated with large foci of heavy hemocytic infiltration in cockles *Cerastoderma edule* from Galicia (NW Spain). *J Invertebr Pathol.* (2003) 84:234–7. doi: 10.1016/j.jip.2003.11.002
89. Rasmussen LPD. Virus-associated granulocytomas in the marine mussel, *Mytilus edulis*, from three sites in Denmark. *J Invertebrate Pathol.* (1986) 48:117–23. doi: 10.1016/0022-2011(86)90150-3
90. Ip HS, Desser SS. A picornavirus-like pathogen of *Cotylogaster occidentalis* (Trematoda: Aspidogastrea), an intestinal parasite of freshwater mollusks. *J Invertebrate Pathol.* (1984) 43:197–206. doi: 10.1016/0022-2011(84)90138-1